

## *Electronic Supplementary Information*

# **Multistimuli-responsive behaviors of a phosphorescent Cu<sub>3</sub>pyrazolate<sub>3</sub> complex for luminescent logic gates and encrypted information transformation**

Wen-Jing Tang,<sup>+</sup> Hu Yang,<sup>+</sup> Su-Kao Peng, Ze-Miao Xiao, Guo-Quan Huang, Ji Zheng<sup>\*</sup> and Dan Li<sup>\*</sup>

<sup>+</sup>W.-J. Tang and H. Yang contributed equally to this work

College of Chemistry and Materials Science, Guangdong Provincial Key Laboratory of Functional Supramolecular Coordination Materials and Applications, Jinan University, Guangzhou 510632, China.

E-mail: jizheng@jnu.edu.cn, danli@jnu.edu.cn

### **Table of Contents**

<b>Experimental details</b> .....	S3-S6
Syntheses and characterization of ligand HL and <b>1</b>	
<b>Fig. S1~S4</b> ( <sup>1</sup> H NMR, FT-IR, PXRD and TGA)	
<b>Crystal Data</b> .....	S7-S8
<b>Table S1-S3</b> (Structure refinement and crystallographic parameters; Selected geometrical parameters)	
<b>Fig. S5</b> (The asymmetric units of complex <b>1</b> )	
<b>Computational Details and photophysical data</b>	
<b>Fig. S6</b> (Colour-filled independent gradient model (IGM) isosurfaces) .....	S9
<b>Fig. S7~S12</b> (Photophysical properties of complex <b>1</b> and ligand HL) .....	S10-S12
<b>Fig. S13~S17</b> (The photographs of <b>1-G</b> after contacted with various organic solvents; PXRD patterns of complex <b>1</b> after grinding or contacted with various organic solvents) .....	S13-S15
<b>Table S4</b> (Photophysical parameters of HL and complex <b>1</b> in different solid states) .....	S16
<b>Table S5~S6</b> (Selected TDDFT results of complex <b>1</b> ) .....	S15-S17
<b>Fig. S18</b> (The optimized geometries of adducts) .....	S18
<b>Table S7</b> (The selected bond lengths and angles of optimized models of adducts) .....	S19
<b>Table S8~S11</b> (Selected TDDFT results based on the optimized models) .....	S20-S22
<b>Table S12</b> (Selected bond lengths (Å) and angles (°) of optimized models) .....	S23
<b>Reference</b> .....	S24-S25

## Experimental Section

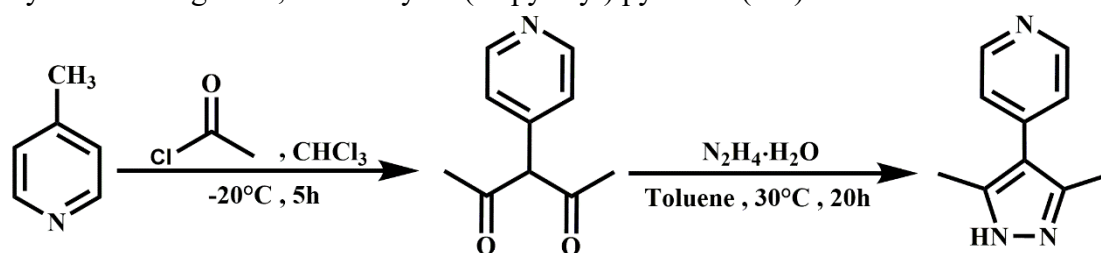
**Materials.** Chemicals and solvents were purchased and used as received without further purification.

### Physical Measurements and Instrumentation

$^1\text{H}$  NMR was recorded in the 400 M Hz. UV-vis absorption spectra were recorded by a Bio-Logic MOS-500 multifunctional circular dichroism spectrometer. Infrared spectra were obtained in KBr disks on a Thermo Scientific FTIR Nicolet is10 spectrometer in the range of  $4000\sim 400\text{ cm}^{-1}$ , and abbreviations used for the IR bands are: w = weak, m = medium, b = broad, s = strong, vs = very strong. Elemental analyses were carried out with an Elementar vario MICRO CUBE equipment. Powder X-ray diffraction (PXRD) experiments were performed on an Rigaku Ultima IV X-ray diffractometer (Cu  $K\alpha$ ,  $\lambda = 1.5418\text{ \AA}$ ) in the step of  $0.02^\circ$  under the conditions 40 KV and 40 mA. Steady-state photoluminescence spectra and emission decay times were recorded by a single-photon counting spectrometer on a Flourolog Horiba spectrofluorometer. Average lifetime ( $\tau_{\text{av}}$ ) were calculated according to the equation:  $\tau_{\text{av}} = [b_1/(b_1+b_2)]*t_1 + [b_2/(b_1+b_2)]*t_2$ . Absolute quantum yield was recorded by Hamamatsu C11347-01 absolute PL quantum yield spectrometer under room temperature. Thermogravimetric analysis curve was recorded by TGA Q50 V20.6 with a heating rate of  $10\text{ }^\circ\text{C/min}$  from  $40$  to  $800\text{ }^\circ\text{C}$  in a  $\text{N}_2$  atmosphere.

### Synthesis and characterization

Synthesis of ligand 3,5-dimethyl-4-(4'-pyridyl) pyrazole (HL)



**Scheme S1.** Synthetic routes to HL.

The ligand was synthesized according to the method described in references,<sup>S1</sup> and its purity was verified by  $^1\text{H}$  nuclear magnetic resonance ( $^1\text{H}$  NMR, Fig. S1), elemental analysis and Fourier transform infrared spectra (FT-IR, Fig. S2). 4-Methylpyridine (18.2 ml, 186 mmol) was dissolved in  $\text{CHCl}_3$  (50 mL) and then the resulting solution was cooled to  $-20^\circ\text{C}$ , followed by the dropwise added acetyl chloride (10.6 ml, 149 mmol) with a separatory funnel while stirring. After stirring for 60 min at  $-20\text{ }^\circ\text{C}$ , the solution turns dark green, affording a brownish-yellow liquid after 3.5 hours, which was distilled under reduced pressure to obtain a brown solid. Then, the brown solid was dissolved in toluene to form a yellow solution and insoluble tan solid, followed by a suction filtration under reduced pressure to removed the solid. Into the resulting yellow filtrate, hydrazine hydrate (4 mL, 80%) is added, and then the reaction mixture was stirred at room temperature for 17 h. The crude products were obtained after removing the solvent under reduced pressure, and furtherly purified by column chromatography (MeOH : Ethyl acetate = 1:40, V:V). Finally, the pure ligands were harvested as the white or pale yellow solid and dried at  $60\text{ }^\circ\text{C}$  in vacuum. Yield: 1.92 g, 5.97% (based

on 4-methylpyridine). The calculated elemental analyses for 3,5-dimethyl-4-(4'-pyridyl) pyrazole HL ( $C_{10}H_{11}N_3$ , %): C, 69.34; H, 6.40; N, 24.26; found: C, 69.44; H, 7.44; N, 23.37. FT-IR data (KBr,  $cm^{-1}$ ): 3309(vs), 3190(vs), 3138(vs), 3085(vs), 1607(vs), 1525(s), 1453(m), 1409(s), 1325(w), 1282(w), 1218(w), 998(vs), 827(vs), 776(s), 700(s), 639(w), 589(w), 553(m).  $^1H$  NMR (400 MHz,  $CD_3SOCD_3$ , 298 K):  $\delta$  (ppm) 8.53 (d, 2H,  $\alpha$ -PyH), 7.32 (d, 2H,  $\beta$ -PyH), 2.26 (s, 6H,  $CH_3$ ).

#### Synthesis of complex **1** ( $Cu_3L_3$ )

The mixture of  $Cu(OH)_2$  (0.015 mmol, 1.5 mg), HL (0.03 mmol, 5.2 mg) and MeOH (3 mL) were sealed in an 8-mm-inside-diameter Pyrex tube, then heated to 140°C for 72 h, followed by the slow cooling down to room temperature with the rate of 5 °C/h in a programmable oven. Colourless needle-like crystals were collected and air-dried. Yield, 2.2 mg, 62.5% based on HL. The calculated elemental analyses for  $Cu_3L_3$  ( $Cu_3C_{30}H_{30}N_9$ , %): C, 50.90; H, 4.24; N, 17.81; found: C, 51.62; H, 4.65; N, 17.24. FT-IR data (KBr,  $cm^{-1}$ ): 3432(vs), 2359(m), 1607(vs), 1523(s), 1432(s), 1375(w), 1223(w), 1277(m), 1048(w), 1015(w), 830(m), 709(m), 667(m), 575(w).

*Caution!* Solvothermal method should be carefully applied. Prior to heating, the volume of solution exceeding one third of the volume of the glass tubes should be prevented to avoid the overflowing. When flame-sealing and opening the glass tubes, the hazards of empyrosis and incised wound should be avoided.

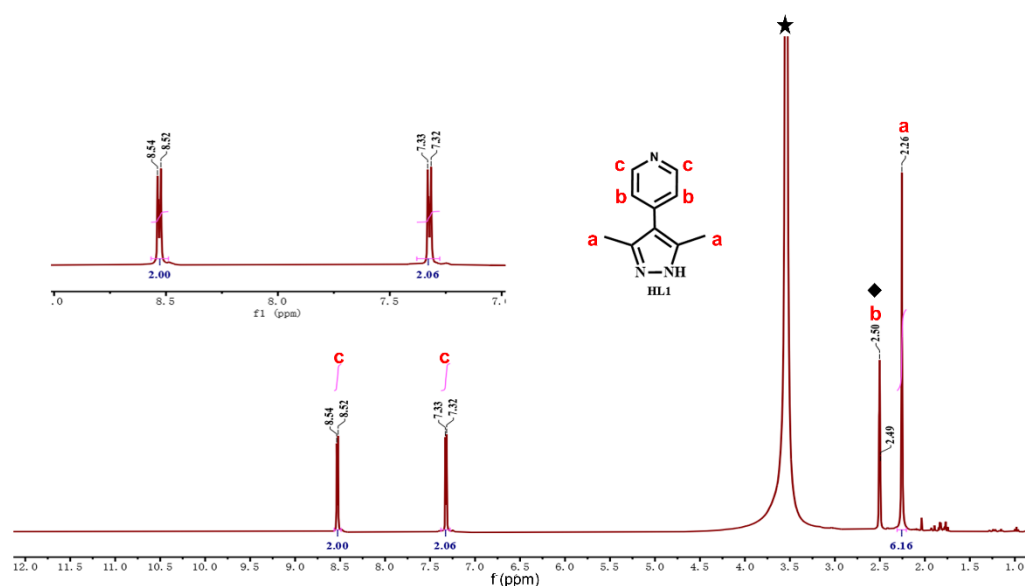


**Fig. S1**  $^1H$  NMR spectrum of HL ( $CD_3SOCD_3$ ). Note that black diamond square belongs to solvent peak and pentagram represents water peak.

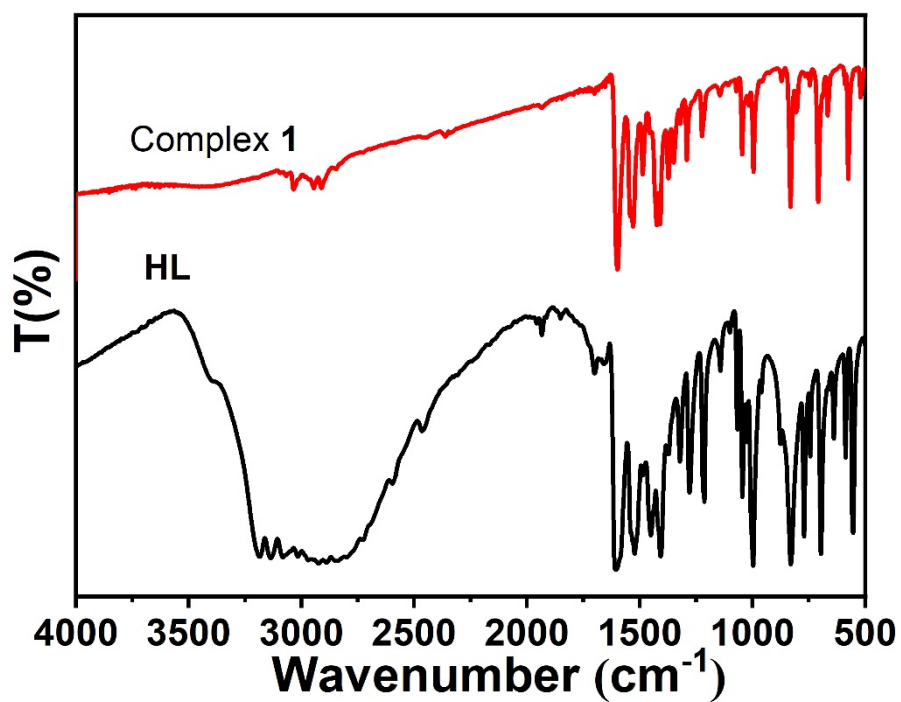


**Fig. S2** FT-IR spectra of complex 1 and HL.

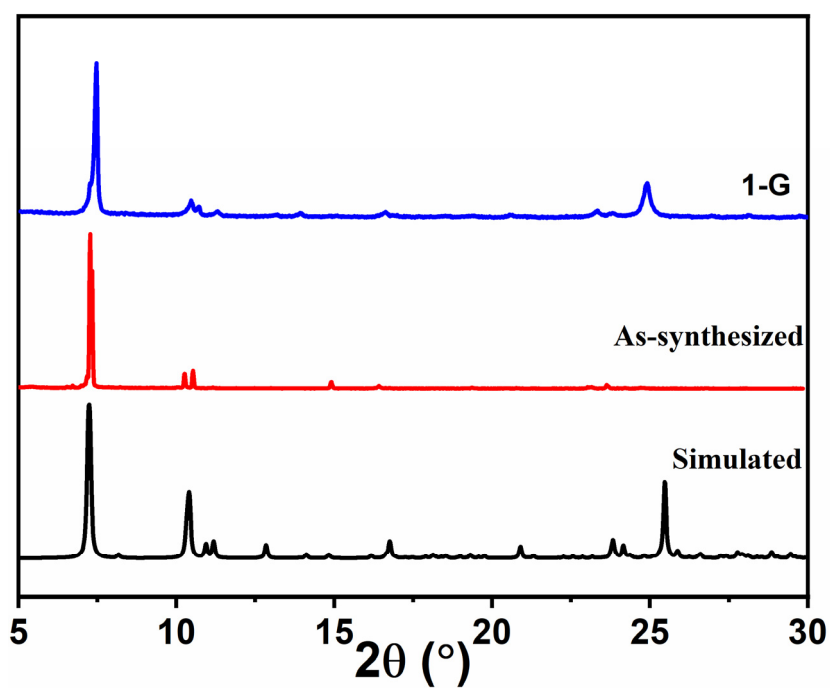


**Fig. S3** PXRD patterns of complex 1 by different treatments.

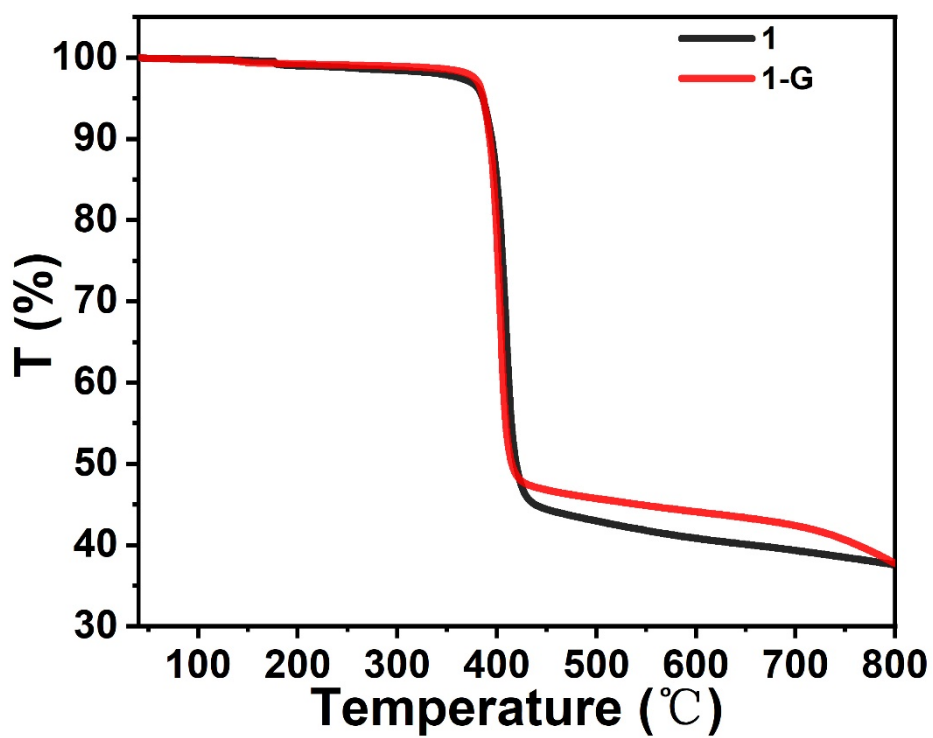


**Fig. S4** Thermal gravimetric curves of complex **1**, **1-G** recorded from 40 °C to 800 °C in nitrogen atmosphere at rate of 10 °C/min.

### X-Ray Crystallography

Suitable single crystals of complex **1** were mounted with glue at the end of a glass fiber. Data collection was performed on an Oxford Diffraction XtalAB [Rigaku(Cu) X-ray dual wavelength source,  $K\alpha$ ,  $\lambda = 1.5418 \text{ \AA}$ ] equipped with a monochromator and CCD plate detector (CrysAlisPro CCD, Oxford Diffraction Ltd) at 100 K, 297.13 K. Structures were solved by direct methods by ShelXS<sup>S2</sup> in Olex2 1.2<sup>S3</sup> and refined on  $F^2$  using full-matrix least-squares (SHELXL-2016/6<sup>S2</sup> in Olex2 1.2<sup>S3</sup>). All non-hydrogen atoms were refined with anisotropic thermal parameters, and all hydrogen atoms were included in calculated positions and refined with isotropic thermal parameters riding on those of the parent atoms. Crystal data and structure refinement parameters are summarized in Table S1. CCDC Nos. 2216799 and 2216800.

**Table S1** Structure refinement and crystallographic parameters of complex **1**.

Temperature (K)	100	297
<b>Empirical formula</b>	C <sub>30</sub> H <sub>30</sub> Cu <sub>3</sub> N <sub>9</sub>	C <sub>30</sub> H <sub>30</sub> Cu <sub>3</sub> N <sub>9</sub>
<b>Formula weight</b>	707.25	707.25
<b>Wavelength (<math>\text{\AA}</math>)</b>	1.54184	1.54184
<b>Crystal system</b>	Triclinic	Triclinic
<b>space group</b>	<i>P</i> -1	<i>P</i> -1
<b><i>a</i> (<math>\text{\AA}</math>)</b>	10.4279(2)	10.4908(3)
<b><i>b</i> (<math>\text{\AA}</math>)</b>	11.6438(2)	11.7213(4)
<b><i>c</i> (<math>\text{\AA}</math>)</b>	11.6569(9)	11.8662(3)
<b><math>\alpha</math> (<math>^\circ</math>)</b>	90.0640(1)	88.781(2)
<b><math>\beta</math> (<math>^\circ</math>)</b>	97.4878(1)	84.156(2)
<b><math>\gamma</math> (<math>^\circ</math>)</b>	91.1987(1)	89.817(3)
<b>Volume (<math>\text{\AA}^3</math>)</b>	1403.01(4)	1451.22(7)
<b><i>Z</i></b>	2	2
<b><math>\rho_{\text{calc}}</math> (g/cm<sup>3</sup>)</b>	5.022	1.619
<b><i>R</i><sub>int</sub></b>	0.0184	0.0668
<b>Completeness (%)</b>	99	98
<b>Goodness-of-fit on <math>F^2</math></b>	1.054	1.238
<b><i>R</i><sub>1</sub><sup>a</sup> [<i>I</i> &gt; 2σ(<i>I</i>)]</b>	0.0314	0.0786
<b><i>wR</i><sub>2</sub><sup>b</sup> (all data)</b>	0.0320	0.3212
<b>Largest diff. peak and hole (e/<math>\text{\AA}^3</math>)</b>	0.41, -0.56	1.04, -0.80

<sup>a</sup> $R_1 = \Sigma|F_o| - |F_c|/\Sigma|F_o|$ , <sup>b</sup> $wR_2 = \{[\Sigma w(F_o^2 - F_c^2)^2]/\Sigma[w(F_o^2)^2]\}^{1/2}$ ;  $w = 1/[\sigma^2(F_o^2) + (aP)^2 + bP]$ , where  $P = [\max(F_o^2, 0) + 2F_c^2]/3$  for all data.

**Table S2** Selected bond lengths (Å) and angles (°) of complex **1**.

100 K			
Cu(1)-N(1)	1.864(4)	Cu(1)-N(6)	1.858(7)
Cu(2)-N(2)	1.863(5)	Cu(2)-N(3)	1.859(8)
Cu(3)-N(4)	1.856(7)	Cu(3)-N(5)	1.857(6)
N(1)-Cu(1)-N(6)	175.62(7)	N(2)-Cu(2)-N(3)	177.80(7)
N(5)-Cu(3)-N(4)	178.10(7)		
297 K			
Cu(1)-N(1)	1.849(7)	Cu(1)-N(6)	1.856(7)
Cu(2)-N(2)	1.862(6)	Cu(2)-N(3)	1.861(6)
Cu(3)-N(4)	1.849(6)	Cu(3)-N(5)	1.855(7)
N(1)-Cu(1)-N(6)	175.1(3)	N(2)-Cu(2)-N(3)	177.8(3)
N(5)-Cu(3)-N(4)	177.5(3)		

**Table S3** The key structural parameters of complex **1** in the single crystals.

Temperature (K)	100	297
$d_{\text{Cu}\cdots\text{Cu, intra}}^{\text{a}}$ (Å)	3.158 - 3.253	3.176 – 3.230
$d_{\text{Cu}\cdots\text{Cu, intra}}^{\text{b}}$ (Å)	3.455	3.434
Cu-N (Å)	1.856 - 1.864	1.849 - 1.862
N-Cu-N (°)	175.6 - 178.1	175.1 - 177.8
Pyridyl – Pyrazyl (°)	24.46	31.42
	28.71	27.23
	46.91	49.12
Pyrazyl - Cu <sub>3</sub> N <sub>6</sub> (°)	4.11	3.36
	5.06	6.09
	9.12	10.74
Pyridyl - Cu <sub>3</sub> N <sub>6</sub> (°)	21.13	28.57
	24.86	24.18
	50.17	52.81

<sup>a</sup>Intramolecular Cu $\cdots$ Cu distance

<sup>b</sup>Intermolecular Cu $\cdots$ Cu distance

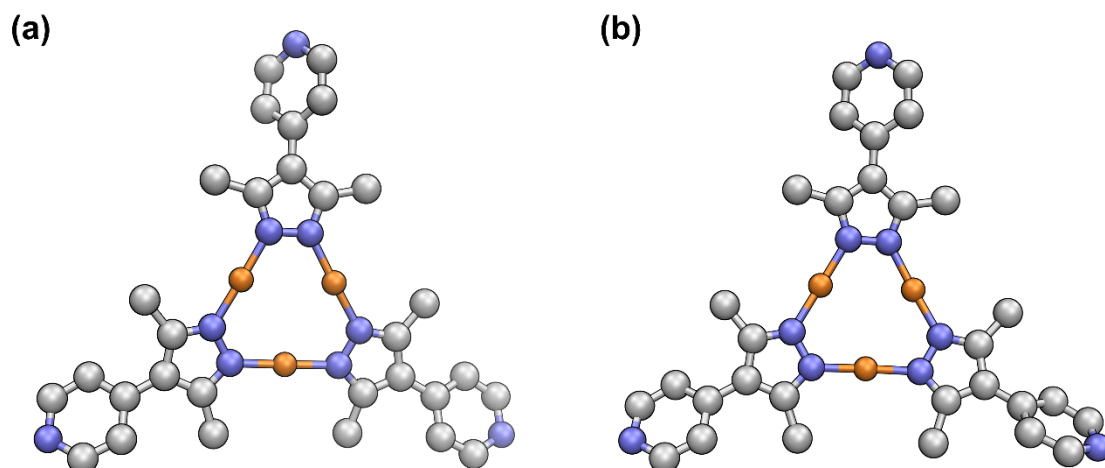


**Fig. S5** The asymmetric units of complex **1** at (a) 100 K, and (b) 297 K. All hydrogen atoms are deleted for clarity. Colour code: Orange: Cu; blue: N; Gray: C.

### Computational Detail and photophysical data

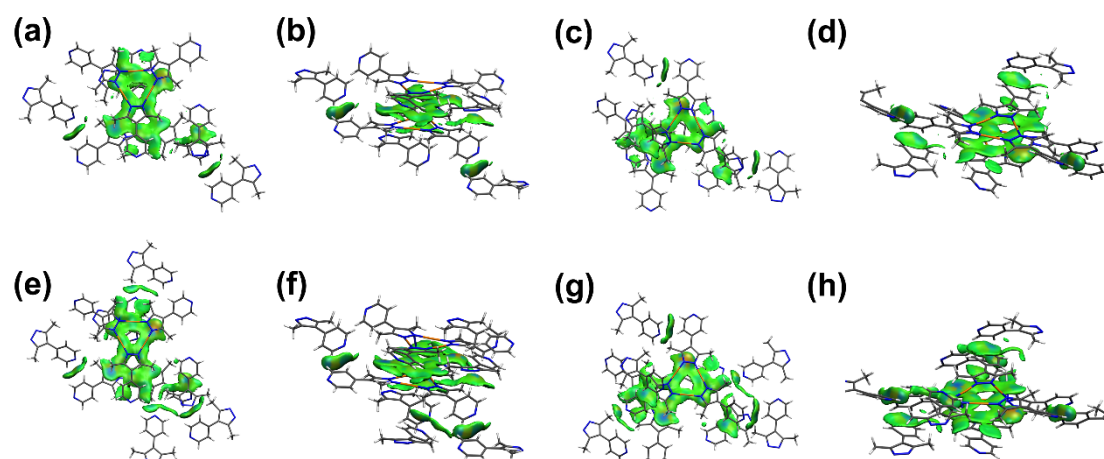
Density functional theory (DFT) and time-dependent DFT (TDDFT) calculations were conducted by Gaussian 09E<sup>S4</sup> software unless otherwise mentioned. The hybrid functional PBE0<sup>S5, S6</sup>-D3<sup>S7</sup>(BJ<sup>S8</sup>) and def-TZVP<sup>S9</sup> basis set were used throughout. The following models were selected and optimized. (1) The monomer of complex **1**. (2) The dimer of complex **1**. (3) CH<sub>2</sub>Cl<sub>2</sub> and CHCl<sub>3</sub> molecules. (4) Four hydrogen- and halogen-bonded 1:1 adducts, i.e., **1**•CHCl<sub>3</sub>(H), **1**•CHCl<sub>3</sub>(Cl), **1**•CH<sub>2</sub>Cl<sub>2</sub>(H), and **1**•CH<sub>2</sub>Cl<sub>2</sub>(Cl). In each adduct, CHCl<sub>3</sub> or CH<sub>2</sub>Cl<sub>2</sub> form a hydrogen or halogen bond with one pyridyl N atoms of complex **1**. (5) A hydrogen-bonded 1:3 adduct, **1**•3CHCl<sub>3</sub>(H), where three CHCl<sub>3</sub> binds with a Cu<sub>3</sub>[4-(pyrid-4'-yl)-3,5-dimethylpyrazolate)]<sub>3</sub> molecule by the hydrogen bonds. After geometrical optimization, the following computations were carried out.

Electrostatic potential (ESP) surfaces were drawn for the monomer of complex **1**, CH<sub>2</sub>Cl<sub>2</sub>, and CHCl<sub>3</sub>, by mapping ESP on the van der Waals isosurfaces of these models with isovalue = 0.001 a.u. Independent gradient model based on Hirshfeld partition (IGMH) and energy decomposition analysis (EDA) were performed for **1**•CHCl<sub>3</sub>(H), **1**•CHCl<sub>3</sub>(Cl), **1**•CH<sub>2</sub>Cl<sub>2</sub>(H), and **1**•CH<sub>2</sub>Cl<sub>2</sub>(Cl). The cubic files (cub) for IGMH analysis were generated by Multiwfn 3.8 software,<sup>S10</sup> and the IGMH inter surfaces were drawn by VMD 1.93 program.<sup>S11</sup> EDA calculations were performed using AMS software.<sup>S12, S13</sup> The dispersion-corrected BLYP<sup>S14-S16</sup>-D3<sup>S7</sup>(BJ<sup>S8</sup>) functional was utilized in EDA calculations, along with the triple-zeta polarization (TZ2P<sup>S17</sup>) basis set with small frozen core approximation.

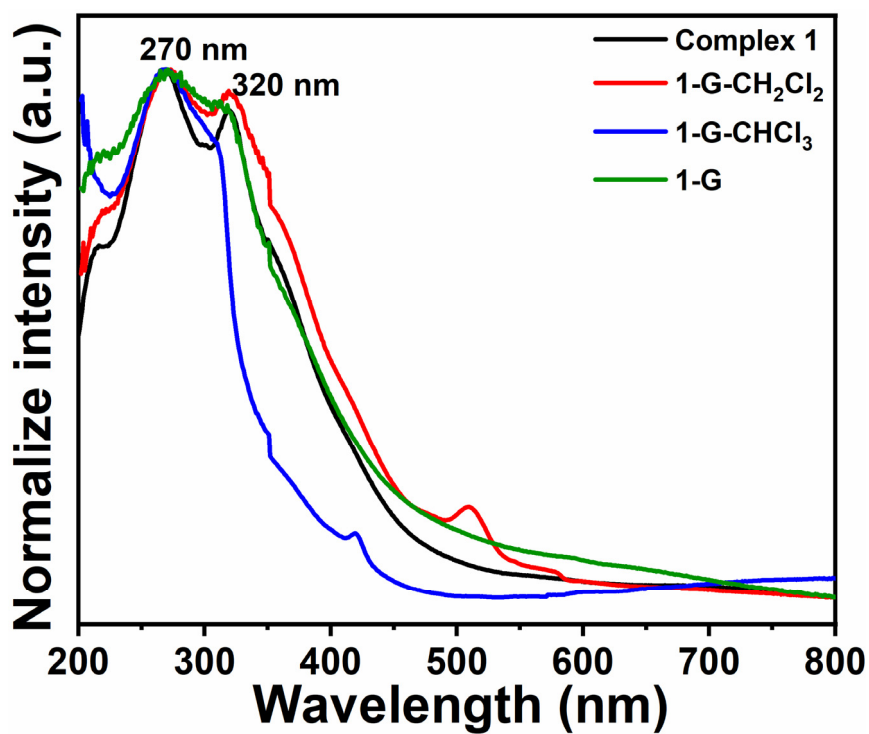
TDDFT calculations were performed for the first 50 single-singlet and singlet-triplet electronic transitions of all models except for CH<sub>2</sub>Cl<sub>2</sub> and CHCl<sub>3</sub>. The result files (fchk and log) were furtherly treated by Multiwfn 3.8 software for extracting the information of electronic transitions, and generating the cubic files (cub) of electron density difference (EDD). The isovalue of EDD maps was 0.0005 a.u. The nature of excited states was clarified by EDD maps (Abbreviation: MMCT = metal-to-metal charge transfer, LMMCT = ligand-to-metal-metal charge transfer, ILCT = intraligand



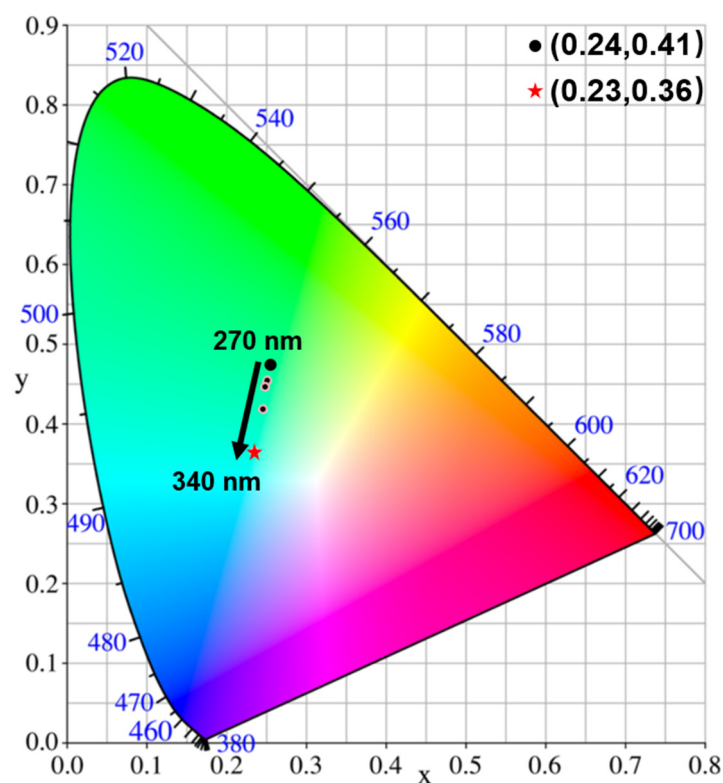
charge transfer, MLCT = metal-to-ligand charge transfer). As summarized in Table S5-S8, the TDDFT results of selected excited states were listed for the four 1:1 adducts. These representative excited states are the lowest singlet and triplet excited states ( $S_1$  and  $T_1$ ), the singlet excited states with the largest oscillator strengths ( $f$ ), and the triplet excited states closest to the  $S_1$  states in energy (i.e., the triplet state with the highest transition energy below that of the first singlet excited state and the triplet state with the lowest transition energy above that of the first singlet excited state). For the monomer of complex **1**, the results of the (near-)degenerated  $S_1$ - $S_3$  states were listed, so were  $T_1$ - $T_3$  states (Table S5). For hydrogen-bonded 1:3 adduct, **1**•3CHCl<sub>3</sub>(H), only the results of  $S_1$  and  $T_1$  states were provided in Table S9.



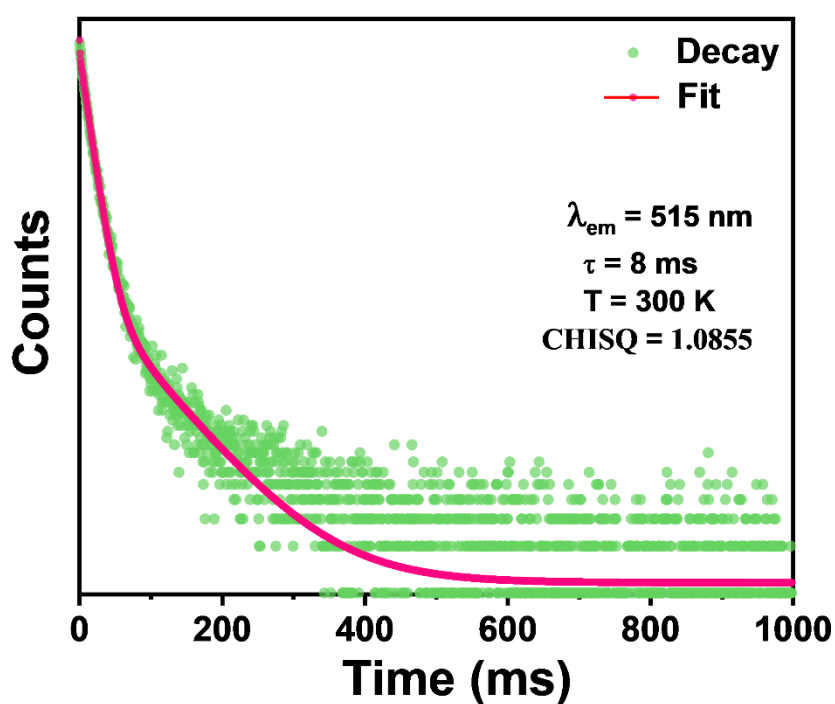
**Fig. S6** Colour-filled independent gradient model (IGM) isosurfaces (Isovalue = 0.005 a.u.) around a central molecule of **1** at (a~d) 300 K, and (e~h) 77 K, observed from the reverse side. Note that green region of IGM isosurfaces indicates the weak attraction at the level of normal van der Waals interactions while cyan region refers to stronger attraction but weaker than standard hydrogen bond.



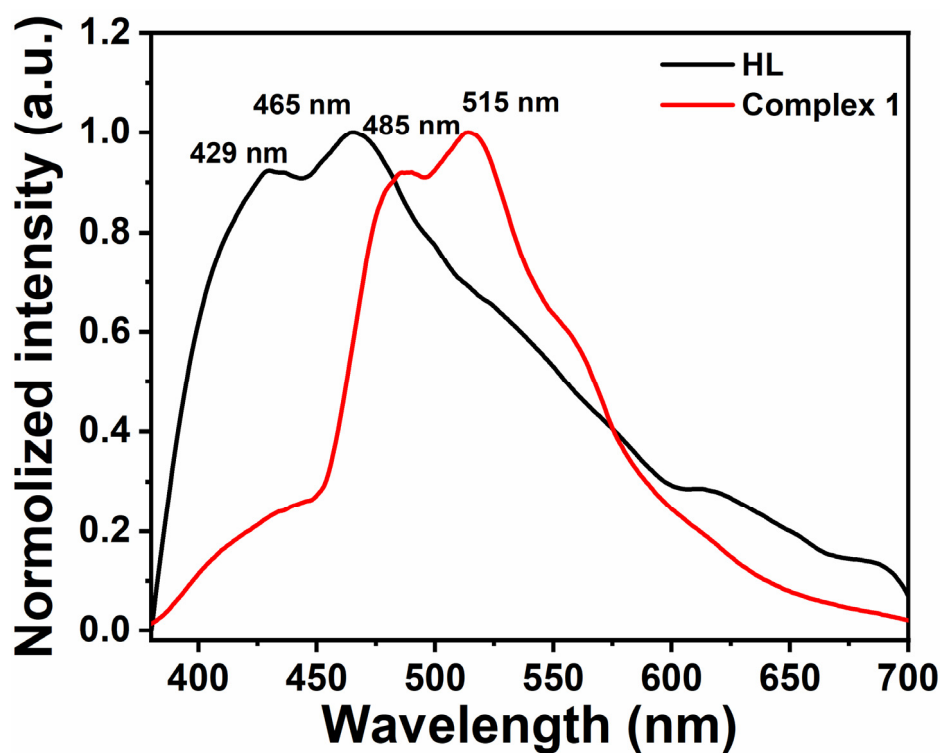
**Fig. S7** Normalized solid-state UV-vis absorption spectra of complex **1** with different treatments.



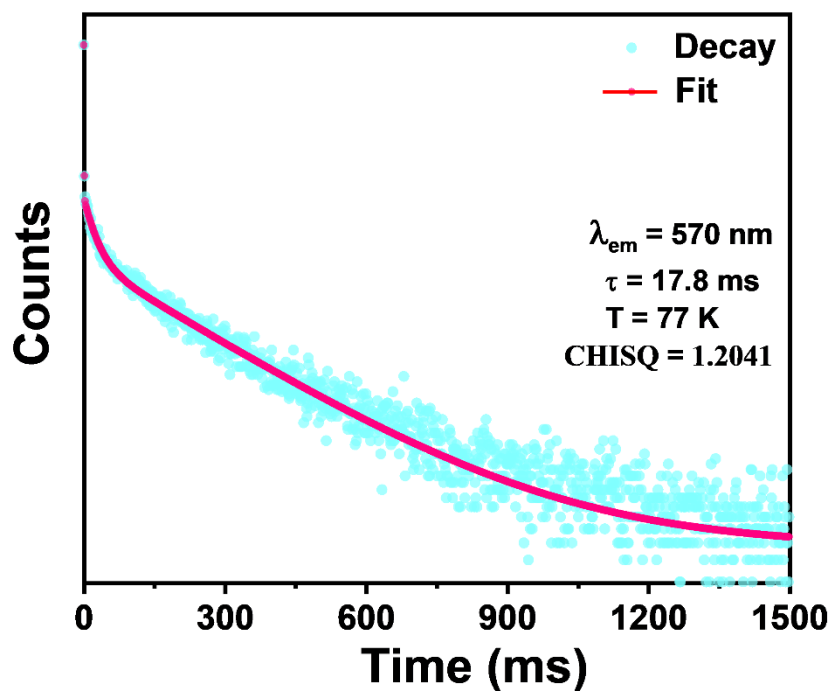
**Fig. S8** Emission colour profile in CIE-1931 Chromaticity diagram of complex **1**, showing data plots of emission spectra with excitation wavelengths increasing from 270 nm to 340 nm along the arrow direction.



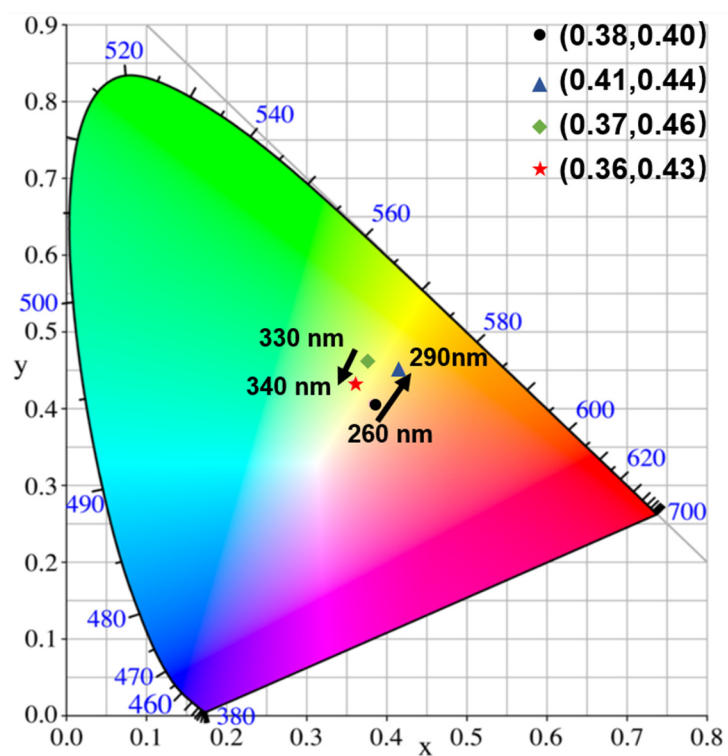
**Fig. S9** Emission decay profiles of crystalline complex **1** at 300 K.



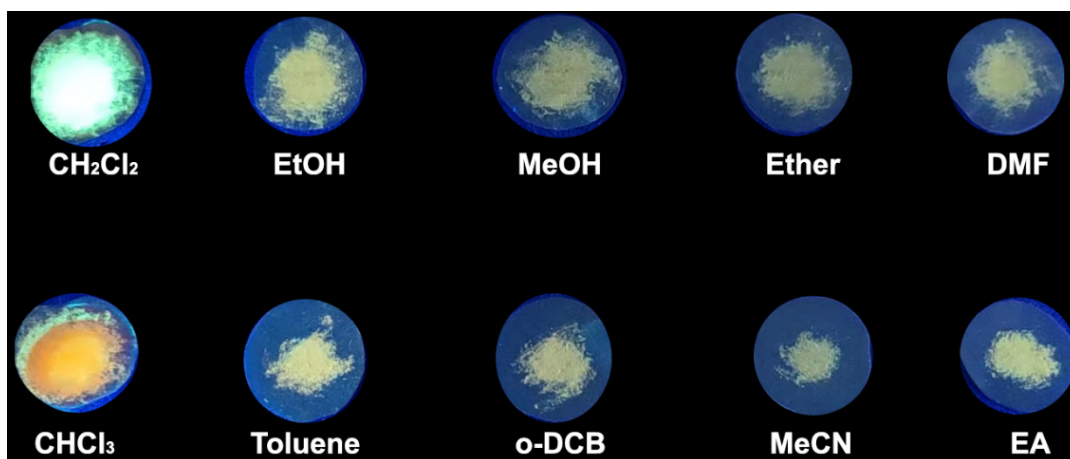
**Fig. S10** Normalized solid-state emission spectra of HL and complex **1** at 300 K (Ex = 320 nm).



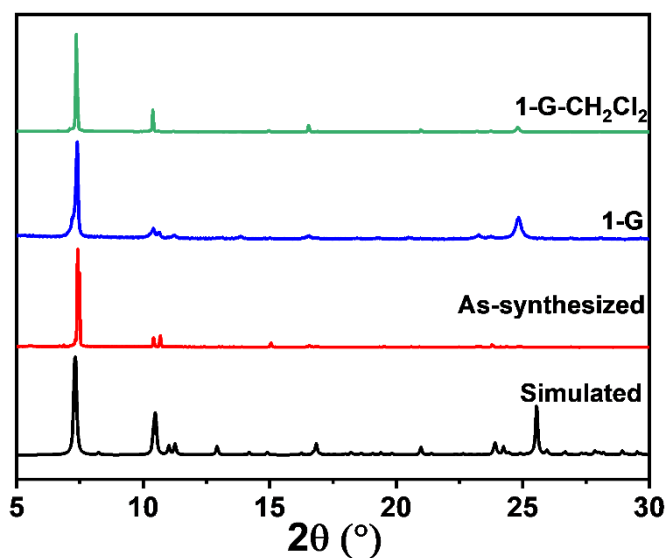
**Fig. S11** Emission decay profiles of crystalline complex **1** at 77 K.



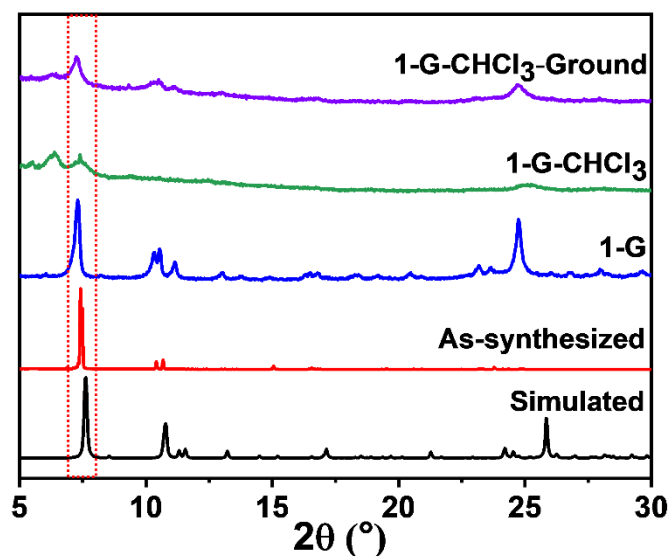
**Fig. S12** CIE chromaticity diagram of **1-G** at different excitation wavelengths.



**Fig. S13** The photographs of **1-G** after dropping with various organic solvents under UV = 254 nm. (o-DCB: o-Dichlorobenzene; EA: Ethyl acetate). Note that the sample was loaded on filter paper sheets.



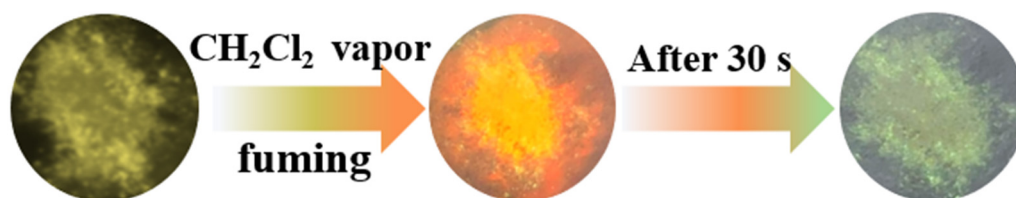
**Fig. S14** PXRD patterns of complex **1**, **1-G** and **1-G-CH<sub>2</sub>Cl<sub>2</sub>** (**1-G**: Ground sample; **1-G-CH<sub>2</sub>Cl<sub>2</sub>**: the **1-G** contact with CH<sub>2</sub>Cl<sub>2</sub> and measured after 60 seconds).



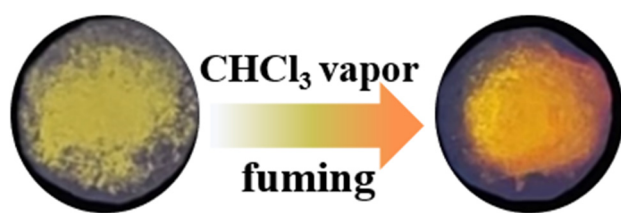
**Fig. S15** PXRD patterns of complex **1**, **1-G** and **1-G-CHCl<sub>3</sub>**, **1-G-CHCl<sub>3</sub>-ground** (**1-G-CHCl<sub>3</sub>**: the **1-G** contacted with CHCl<sub>3</sub> and measured after 60 seconds. **1-G-CHCl<sub>3</sub>-Ground**: the **1-G-CHCl<sub>3</sub>** was ground and measured). The red frame indicating the transformation of peak at 7.23° after corresponding treatment.

**Table S4** Photophysical parameters HL and complex **1** in different solid states.

Compound	State	$\lambda_{\text{ex}}$ (nm)	$\lambda_{\text{em}}$ (nm)	$\lambda_{\text{abs}}$ (nm)	$\tau$ (ms)	QY (%)
HL	Powder	320	570,465,430		-	-
<b>1</b> (300 K)	Crystal	320	515,485	270,320	5.2,17,10	2.8
<b>1</b> (77 K)	Crystal	303	565,525	-	28	-
<b>1-G</b>	Powder	320	650,560,420	270,310	15.7	3.2
<b>1-G-CH<sub>2</sub>Cl<sub>2</sub></b>	Powder	320	515, 485	270,320		-
<b>1-G-CHCl<sub>3</sub></b>	Powder	320	655	270,310		-

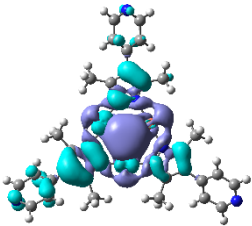
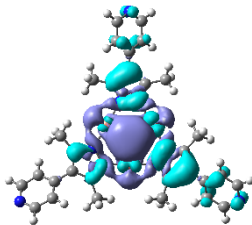
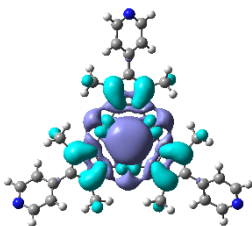
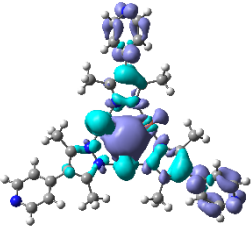
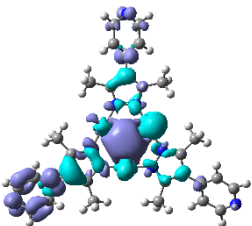


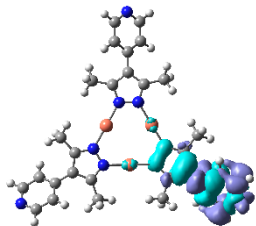
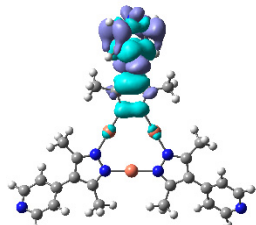
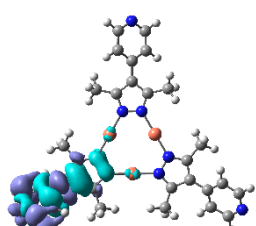
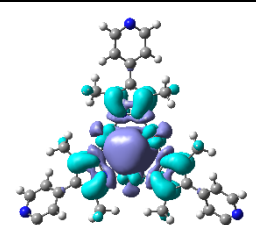
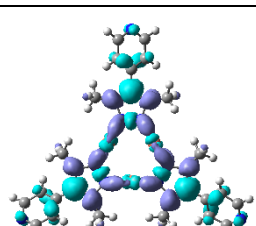
**Fig. S16** The photographs of **1-G** on filter paper sheets after fumigate with CH<sub>2</sub>Cl<sub>2</sub> (UV = 254 nm).



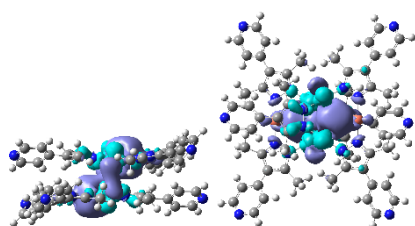
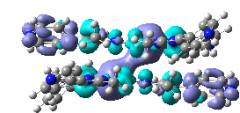
**Fig. S17** The photographs **1-G** on filter paper sheets and fumigating with  $\text{CHCl}_3$  (UV = 254 nm).

**Table S5** Selected TDDFT results of singlet-singlet spin-allowed transitions and singlet-triplet spin-forbidden transitions based on the optimized monomer of complex **1**.

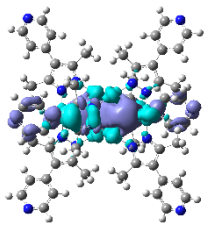
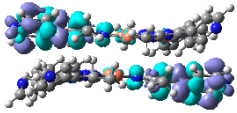
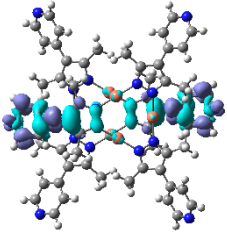
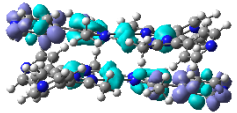
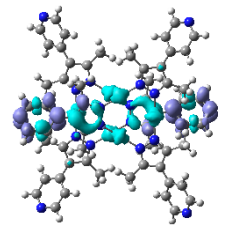
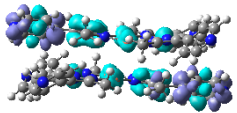
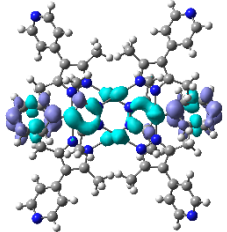
Item	E (eV)	$\lambda$ (nm)	$f$	EDD	Assignment
S <sub>1</sub>	4.565	271.6	0.002		$^1\text{MMCT}/^1\text{LMMCT}$
S <sub>2</sub>	4.565	271.6	0.002		$^1\text{MMCT}/^1\text{LMMCT}$
S <sub>3</sub>	4.682	264.8	0.000		$^1\text{MMCT}$
S <sub>4</sub>	4.735	261.9	0.431		$^1\text{ILCT}/^1\text{MLCT}/^1\text{MMCT}$
S <sub>5</sub>	4.735	261.8	0.432		$^1\text{ILCT}/^1\text{MLCT}/^1\text{MMCT}$

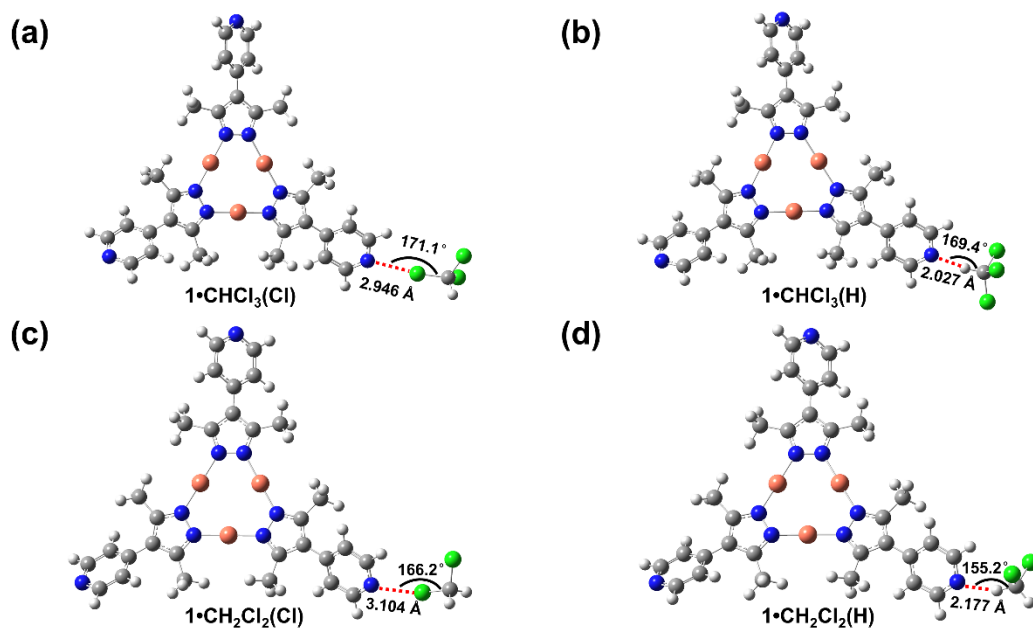
T <sub>1</sub>	3.540	350.2	0.000		<sup>3</sup> ILCT/ <sup>3</sup> MLCT
T <sub>2</sub>	3.541	350.1	0.000		<sup>3</sup> ILCT/ <sup>3</sup> MLCT
T <sub>3</sub>	3.542	350.0	0.000		<sup>3</sup> ILCT/ <sup>3</sup> MLCT
T <sub>21</sub>	4.564	271.7	0.000		<sup>1</sup> MMCT/ <sup>1</sup> LMMCT
T <sub>22</sub>	4.613	268.8	0.000		<sup>3</sup> ILCT/ <sup>3</sup> MLCT

**Table S6** Selected TDDFT results of singlet-singlet spin-allowed transitions and singlet-triplet spin-forbidden transitions based on the optimized dimer of complex **1**.

Item	E (eV)	$\lambda$ (nm)	$f$	EDD <sup>a</sup>	Assignment
S <sub>1</sub>	4.332	286.2	0.000		<sup>1</sup> MMCT/ <sup>1</sup> LMMCT
S <sub>3</sub> <sup>b</sup>	4.444	279.0	0.332		<sup>1</sup> ILCT/ <sup>1</sup> MLCT/ <sup>1</sup> MMCT



					
T <sub>1</sub>	3.452	359.2	0.000	 	<sup>3</sup> ILCT/ <sup>3</sup> MLCT
T <sub>25</sub>	4.326	286.6	0.000	 	<sup>3</sup> ILCT/ <sup>3</sup> MLCT
T <sub>26</sub>	4.347	285.2	0.000	 	<sup>3</sup> ILCT/ <sup>3</sup> MLCT

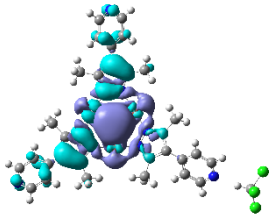
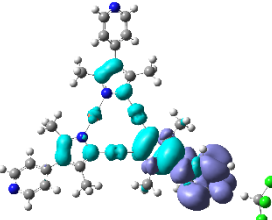
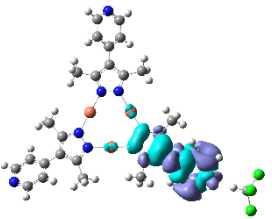
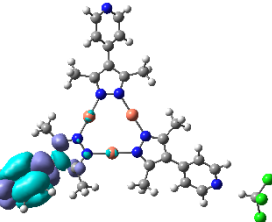
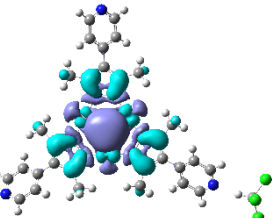


**Fig. S18** The optimized geometries of adducts (a)  $1\bullet\text{CHCl}_3(\text{Cl})$ , (b)  $1\bullet\text{CHCl}_3(\text{H})$ , (c)  $1\bullet\text{CH}_2\text{Cl}_2(\text{Cl})$  and  $1\bullet\text{CH}_2\text{Cl}_2(\text{H})$ .

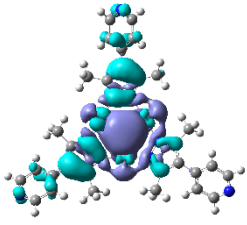
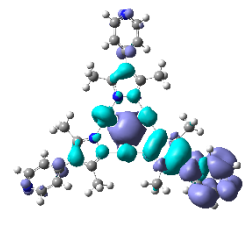
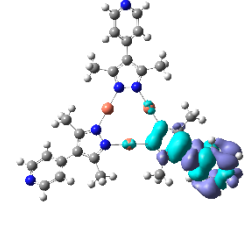
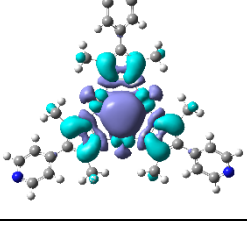
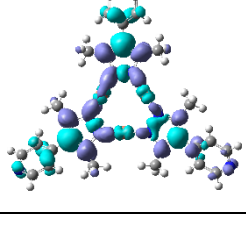
**Table S7** The selected bond lengths and angles of optimized models of  $1\bullet\text{CHCl}_3(\text{X})$  ( $\text{X} = \text{Cl}/\text{H}$ ), and  $1\bullet\text{CH}_2\text{Cl}_2(\text{X})$  ( $\text{X} = \text{Cl}/\text{H}$ ).

Item	$d(\text{N}\cdots\text{X})$ (Å)	$\text{N}\cdots\text{X}-\text{C}$ (°)	Torsion angle (°)
$1\bullet\text{CHCl}_3(\text{Cl})$	2.946	171.1	38.1
			39.3
			38.6
$1\bullet\text{CHCl}_3(\text{H})$	2.027	169.4	37.8
			38.9
			39.5
$1\bullet\text{CH}_2\text{Cl}_2(\text{Cl})$	3.104	166.2	38.8
			39.0
			39.1
$1\bullet\text{CH}_2\text{Cl}_2(\text{H})$	2.177	155.2	37.8
			38.7
			39.3

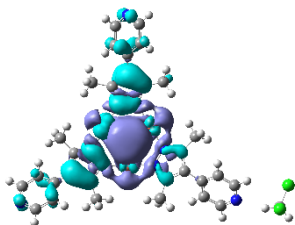
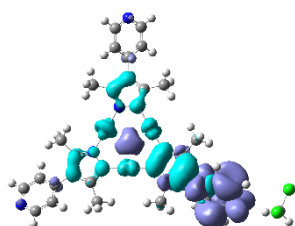
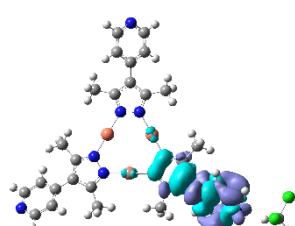
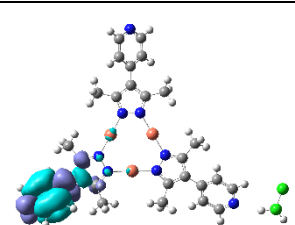
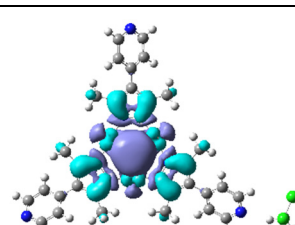
**Table S8** Selected TDDFT results of singlet-singlet spin-allowed transitions and singlet-triplet spin-forbidden transitions based on the optimized **1•CHCl<sub>3</sub>(H)**.

Item	E (eV)	$\lambda$ (nm)	$f$	EDD	Assignment
S <sub>1</sub>	4.548	272.6	0.009		<sup>1</sup> MMCT/ <sup>1</sup> LMMCT
S <sub>3</sub>	4.610	268.9	0.654		<sup>1</sup> ILCT/ <sup>1</sup> MLCT
T <sub>1</sub>	3.507	353.5	0.000		<sup>3</sup> ILCT
T <sub>21</sub>	4.536	273.3	0.000		<sup>3</sup> ILCT
T <sub>22</sub>	4.568	271.4	0.000		<sup>3</sup> MMCT

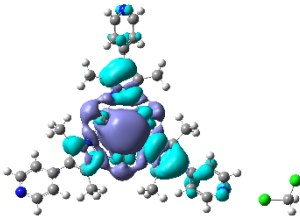
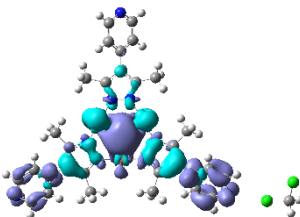
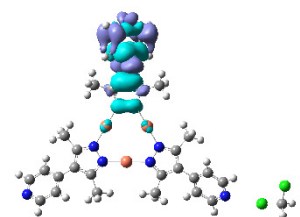
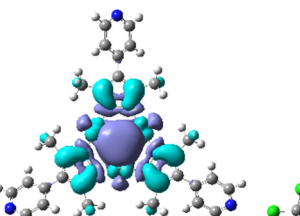
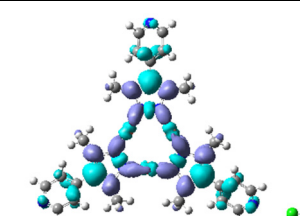
**Table S9** Selected TDDFT results of singlet-singlet spin-allowed transitions and singlet-triplet spin-forbidden transitions based on the optimized **1•CHCl<sub>3</sub>(Cl)**.

Item	E (eV)	$\lambda$ (nm)	$f$	EDD	Assignment
S <sub>1</sub>	4.560	271.9	0.003		<sup>1</sup> MMCT/ <sup>1</sup> LMMCT
S <sub>4</sub>	4.709	263.3	0.781		<sup>1</sup> MMCT/ <sup>1</sup> ILCT
T <sub>1</sub>	3.530	351.3	0.000		<sup>3</sup> ILCT
T <sub>21</sub>	4.565	271.6	0.000		<sup>3</sup> MMCT
T <sub>22</sub>	4.613	268.8	0.000		<sup>3</sup> ILCT/ <sup>3</sup> MLCT

**Table S10** Selected TDDFT results of singlet-singlet spin-allowed transitions and singlet-triplet spin-forbidden transitions based on the optimized **1•CH<sub>2</sub>Cl<sub>2</sub>(H)**.

Item	E (eV)	$\lambda$ (nm)	$f$	EDD	Assignment
S <sub>1</sub>	4.556	272.2	0.004		<sup>1</sup> MMCT/ <sup>1</sup> LMMCT
S <sub>3</sub>	4.673	265.3	0.693		<sup>1</sup> MMCT/ <sup>1</sup> ILCT
T <sub>1</sub>	3.519	352.3	0.000		<sup>3</sup> ILCT
T <sub>20</sub>	4.536	273.3	0.000		<sup>3</sup> ILCT
T <sub>21</sub>	4.566	271.5	0.000		<sup>3</sup> MMCT

**Table S11** Selected TDDFT results of singlet-singlet spin-allowed transitions and singlet-triplet spin-forbidden transitions based on the optimized **1•CH<sub>2</sub>Cl<sub>2</sub>(Cl)**.

Item	E (eV)	$\lambda$ (nm)	$f$	EDD	Assignment
S <sub>1</sub>	4.562	271.8	0.003		<sup>1</sup> MMCT
S <sub>4</sub>	4.732	262.0	0.523		<sup>1</sup> MMCT/ <sup>1</sup> ILCT
T <sub>1</sub>	3.540	350.2	0.000		<sup>3</sup> ILCT
T <sub>21</sub>	4.536	273.4	0.000		<sup>3</sup> MMCT
T <sub>22</sub>	4.563	271.7	0.000		<sup>3</sup> ILCT/ <sup>3</sup> MLCT

**Table S12** Selected bond lengths (Å) and angles (°) of optimized models.

Item	d(Cu-Cu) (Å)	d(Cu-N) (Å)	N-Cu-N (°)	Torsion angle <sup>a</sup> (°)
1(S <sub>0</sub> )	3.218	1.873	179.6	39.1 <sup>b</sup>
				39.2
				38.9
1(T <sub>1</sub> )	3.219-3.203	1.872-1.875	179.0-179.9	39.5 <sup>b</sup>
				14.2
				39.5
1•CHCl <sub>3</sub> (Cl) (S <sub>0</sub> )	3.216-3.219	1.873-1.873	179.5-179.6	38.1 <sup>b</sup>
				39.3
				38.6
1•CHCl <sub>3</sub> (Cl) (T <sub>1</sub> )	3.205-3.220	1.872-1.876	179.0-179.8	14.6 <sup>b</sup>
				39.6
				39.4
1•CH <sub>2</sub> Cl <sub>2</sub> (Cl) (S <sub>0</sub> )	3.217-3.218	1.873-1.873	179.5-179.6	38.8 <sup>b</sup>
				39.1
				39.0
1•CH <sub>2</sub> Cl <sub>2</sub> (Cl) (T <sub>1</sub> )	3.204-3.221	1.872-1.875	178.9-179.9	39.4 <sup>b</sup>
				14.9
				39.6
1•CHCl <sub>3</sub> (H) (S <sub>0</sub> )	3.217-3.219	1.872-1.874	179.5-179.6	37.8 <sup>b</sup>
				38.9
				39.5
1•CHCl <sub>3</sub> (H) (T <sub>1</sub> )	3.217-3.221	1.871-1.875	178.9-179.9	38.7 <sup>b</sup>
				39.5
				13.5
1•CH <sub>2</sub> Cl <sub>2</sub> (H) (S <sub>0</sub> )	3.217-3.219	1.873-1.874	179.5-179.6	37.8 <sup>b</sup>
				38.7
				39.3
1•CH <sub>2</sub> Cl <sub>2</sub> (H) (T <sub>1</sub> )	3.205-3.219	1.871-1.875	179.0-179.8	15.6 <sup>b</sup>
				39.5
				39.8

<sup>a</sup> Torsion angle between pyridyl and pyrazolyl<sup>b</sup> Refer to the pyridyl which has interaction with CH<sub>2</sub>Cl<sub>2</sub> or CHCl<sub>3</sub>

## Reference

- S1. Q. Cui, X.-Y. Cao and L.-F. Tang, Diorganotin(IV) derivatives containing the 3,5-dimethyl-4-(4'-pyridyl)pyrazole ligand, *Polyhedron*, 2005, **24**, 209-214.
- S2. G. Sheldrick, A short history of SHELX, *Acta Cryst.*, 2008, **64**, 112-122.
- S3. O. V. Dolomanov, L. J. Bourhis, R. J. Gildea, J. A. K. Howard and H. Puschmann, OLEX2: a complete structure solution, refinement and analysis program, *J. Appl. Crystallogr.*, 2009, **42**, 339-341.
- S4. M. J. Frisch, G. W. Trucks, H. B. Schlegel, G. E. Scuseria, M. A. Robb, J. R. Cheeseman, G. Scalmani, V. Barone, G. A. Petersson, H. Nakatsuji, X. Li, M. Caricato, A. V. Marenich, J. Bloino, B. G. Janesko, R. Gomperts, B. Mennucci, H. P. Hratchian, J. V. Ortiz, A. F. Izmaylov, J. L. Sonnenberg, Williams, F. Ding, F. Lipparini, F. Egidi, J. Goings, B. Peng, A. Petrone, T. Henderson, D. Ranasinghe, V. G. Zakrzewski, J. Gao, N. Rega, G. Zheng, W. Liang, M. Hada, M. Ehara, K. Toyota, R. Fukuda, J. Hasegawa, M. Ishida, T. Nakajima, Y. Honda, O. Kitao, H. Nakai, T. Vreven, K. Throssell, J. A. Montgomery Jr., J. E. Peralta, F. Ogliaro, M. J. Bearpark, J. J. Heyd, E. N. Brothers, K. N. Kudin, V. N. Staroverov, T. A. Keith, R. Kobayashi, J. Normand, K. Raghavachari, A. P. Rendell, J. C. Burant, S. S. Iyengar, J. Tomasi, M. Cossi, J. M. Millam, M. Klene, C. Adamo, R. Cammi, J. W. Ochterski, R. L. Martin, K. Morokuma, O. Farkas, J. B. Foresman and D. J. Fox, Gaussian 09, Revision E.01., 2009.
- S5. J. P. Perdew, K. Burke and M. Ernzerhof, Generalized gradient approximation made simple, *Phys. Rev. Lett.*, 1996, **77**, 3865-3868.
- S6. J. P. Perdew, K. Burke and M. Ernzerhof, Generalized gradient approximation made simple [Phys. Rev. Lett. 77, 3865 (1996)], *Phys. Rev. Lett.*, 1997, **78**, 1396-1396.
- S7. S. Grimme, J. Antony, S. Ehrlich and H. Krieg, A consistent and accurate ab initio parametrization of density functional dispersion correction (DFT-D) for the 94 elements H-Pu, *J. Chem. Phys.*, 2010, **132**, 154104.
- S8. S. Grimme, S. Ehrlich and L. Goerigk, Effect of the damping function in dispersion corrected density functional theory, *J. Comput. Chem.*, 2011, **32**, 1456-1465.
- S9. A. Schäfer, C. Huber and R. Ahlrichs, Fully optimized contracted Gaussian basis sets of triple zeta valence quality for atoms Li to Kr, *J. Chem. Phys.*, 1994, **100**, 5829-5835.
- S10. T. Lu and F. Chen, Multiwfn: a multifunctional wavefunction analyzer, *J. Comput. Chem.*, 2012, **33**, 580-592.
- S11. W. Humphrey, A. Dalke and K. Schulten, VMD: Visual molecular dynamics, *J. Mol. Graphics*, 1996, **14**, 33-38.
- S12. G. te Velde, F. M. Bickelhaupt, E. J. Baerends, C. Fonseca Guerra, S. J. A. van Gisbergen, J. G. Snijders and T. Ziegler, Chemistry with ADF, *J. Comput. Chem.*, 2001, **22**, 931-967.
- S13. C. Fonseca Guerra, J. G. Snijders, G. te Velde and E. J. Baerends, Towards an order-N DFT method, *Theor. Chem. Acc.*, 1998, **99**, 391-403.
- S14. A. D. Becke, Density-functional exchange-energy approximation with correct asymptotic behavior, *Phys. Rev. A*, 1988, **38**, 3098-3100.
- S15. C. Lee, W. Yang and R. G. Parr, Development of the Colle-Salvetti correlation-energy formula into a functional of the electron density, *Phys. Rev. B*, 1988, **37**, 785-789.
- S16. B. Miehlich, A. Savin, H. Stoll and H. Preuss, Results obtained with the correlation energy density functionals of Becke and Lee, Yang and Parr, *Chem. Phys. Lett.*, 1989, **157**, 200-206.
- S17. K. L. Bak, P. Jørgensen, T. Helgaker, K. Ruud and H. J. A. Jensen, Gauge-origin independent



multiconfigurational self-consistent-field theory for vibrational circular dichroism, *J. Chem. Phys.*, 1993, **98**, 8873-8887.